Mapping molecular statistics with balanced super-resolution optical fluctuation imaging (bSOFI)

Stefan Geissbuehler* , Noelia L Bocchio , Claudio Dellagiacoma , Corinne Berclaz , Marcel Leutenegger and Theo Lasser

Laboratoire d'Optique Biomédicale, École Polytechnique Fédérale de Lausanne, 1015 Lausanne, Switzerland

Email: Stefan Geissbuehler*- stefan.geissbuehler@epfl.ch; Noelia L Bocchio - noelia.bocchio@epfl.ch; Claudio Dellagiacoma - claudio.dellagiacoma@gmail.com; Corinne Berclaz - corinne.berclaz@epfl.ch; Marcel Leutenegger - marcel.leutenegger@epfl.ch; Theo Lasser - theo.lasser@epfl.ch;

*Corresponding author

Abstract

Background Super-resolution optical fluctuation imaging (SOFI) achieves 3D super-resolution by computing temporal cumulants or spatio-temporal cross-cumulants of stochastically blinking fluorophores. In contrast to localization microscopy, SOFI is compatible with weakly emitting fluorophores and a wide range of blinking conditions. The main drawback of SOFI is the nonlinear response to brightness and blinking heterogeneities in the sample, which limits the use of higher cumulant orders for improving the resolution.

Balanced super-resolution optical fluctuation imaging (bSOFI) analyses several cumulant orders for extracting molecular parameter maps, such as molecular state lifetimes, concentration and brightness distributions of fluorophores within biological samples. Moreover, the estimated blinking statistics are used to balance the image contrast, i.e. linearize the brightness and blinking response and to obtain a resolution improving linearly with the cumulant order.

Results Using a widefield total-internal-reflection (TIR) fluorescence microscope, we acquired image sequences of fluorescently labelled microtubules in fixed HeLa cells. We demonstrate an up to five-fold resolution improvement as compared to the diffraction-limited image, despite low single-frame signal-to-noise ratios. Due to the TIR illumination, the intensity profile in the sample decreases exponentially along the optical axis, which is reported by the estimated spatial distributions of the molecular brightness as well as the blinking on-ratio. Therefore, TIR-bSOFI also encodes depth information through these parameter maps.

Conclusions bSOFI is an extended version of SOFI that cancels the nonlinear response to brightness and blinking heterogeneities. The obtained balanced image contrast significantly enhances the visual perception of super-resolution based on higher-order cumulants and thereby facilitates the access to higher resolutions. Furthermore, bSOFI provides microenvironment-related molecular parameter maps and paves the way for functional super-resolution microscopy based on stochastic switching.

Keywords

fluorescence microscopy — super-resolution — stochastic switching — sofi — cumulants — balanced contrast — molecular statistics — functional imaging

Background

The spatial resolution in classical optical microscopes is limited by diffraction to about half the wavelength of light. During the last two decades, several super-resolution concepts have been developed. Based on the on-off-switching of fluorescent probes, these concepts overcome the diffraction limit by up to an order of magnitude [1]. A straightforward method consists of digitally post-processing an image sequence of stochastically blinking emitters acquired with a standard wide-field fluorescence microscope. Densely packed single fluorophores can be distinguished in time by using high-precision localization algorithms, used for instance in photo-activation localization microscopy (PALM) [2, 3] and stochastic optical reconstruction microscopy (STORM) [4, 5], or by analysing the statistics of the temporal fluctuations as exploited in super-resolution optical fluctuation imaging (SOFI) [6, 7]. SOFI is based on a pixel-wise auto- or cross-cumulant analysis, which yields a resolution enhancement growing with the cumulant order in all three dimensions [6]. Uncorrelated noise, stationary background, as well as out-of-focus light are greatly reduced by the cumulants analysis. While PALM and STORM are commonly based on a frame-by-frame analysis of images of individual fluorophores, SOFI processes the entire image sequence at once and therefore presents significant advantages in terms of the number of required photons per fluorophore and image, as well as in acquisition time [8]. Localization microscopy requires a meta-stable dark state for imaging individual fluorophores [9]. In contrast, SOFI relies solely on stochastic, reversible and temporally resolvable fluorescence fluctuations almost regardless of the on-off duty cycle [8]. The main drawback of SOFI is the amplification of heterogeneities in molecular brightness and blinking statistics which limits the use of higher-order cumulants and therefore resolution. In this article, we revisited the original SOFI concept and propose a reformulation called balanced super-resolution optical fluctuation imaging (bSOFI), which in addition to improving structural details opens a new functional dimension to stochastic switching-based super-resolution imaging. bSOFI allows the extraction of the super-resolved spatial distribution of molecular statistics, such as the on-time ratio, the brightness and the concentration of fluorophores by combining several cumulant orders. Moreover, this information can be used to balance the image contrast in order to compensate for the nonlinear brightness and blinking response of conventional SOFI images. Consequently, bSOFI enables higher-order cumulants to be used and thereby achieves higher resolutions.

Methods

Theory and algorithm

SOFI is based on the computation of temporal cumulants or spatio-temporal cross-cumulants. Cumulants are a statistical measure related to moments. Because cumulants are additive, the cumulant of a sum of independently fluctuating fluorophores corresponds to the sum of the cumulant of each individual fluorophore. This leads to a point-spread function raised to the power of the cumulant order n and therefore a resolution improvement of $\sqrt{n}$, respectively almost n with subsequent Fourier filtering [7]. So far, SOFI has been used exclusively to improve structural details in an image [6, 7, 10]. Information about the on-time ratio, the molecular brightness and the concentration has to our knowledge never been exploited before and therefore represents a new potential for super-resolved imaging.

In the most general sense, the cumulant of order n of a pixel set $\mathbb{P} = \{\vec{r}_1, \vec{r}_2, ..., \vec{r}_n\}$ with time lags $\vec{\tau} = \{\tau_1, \tau_2, ..., \tau_n\}$ can be calculated as [11]

$$\kappa_n\left(\vec{r} = \frac{1}{n}\sum_{i=1}^{n}\vec{r}_i; \vec{\tau}\right) = \sum_{P}(-1)^{|P|-1}(|P|-1)! \prod_{p\in P}\left\langle\prod_{i\in p} I(\vec{r}_i, t-\tau_i)\right\rangle_t , \quad (1)$$

where $\langle ... \rangle_t$ stands for averaging over the time t. P runs over all partitions of a set $\mathbb{S} = \{1, 2, ..., n\}$, which means all possible divisions of $\mathbb{S}$ into non-overlapping and non-empty subsets or parts that cover all elements of $\mathbb{S}$. $|P|$ denotes the number of parts of partition P and p enumerates these parts. $I(\vec{r}_i, t)$ is the intensity distribution measured over time on a detector pixel $\vec{r}_i$. We used the cross-cumulant approach without repetitions to increase the pixel grid density and eliminate any bias arising from noise contributions in auto-cumulants [8]. A 4x4 neighborhood around every pixel was considered to compute all possible n-pixel combinations excluding pixel repetitions. For computational reasons, we

kept only a single combination featuring the shortest sum of distances with respect to the corresponding output pixel $\vec{r} = \frac{1}{n}\sum_{i=1}^{n}\vec{r}_i$. For even better signal-to-noise ratios, it would be beneficial to average over multiple combinations per output pixel. The heterogeneity in output pixel weighting arising from the different pixel combinations has been accounted for by the distance factor as described in [7].

Considering a sample composed of M independently fluctuating fluorophores and assuming a simple two-state blinking model (with characteristic lifetimes $\tau_{\mathrm{on}}, \tau_{\mathrm{off}}$) with slowly varying molecular parameters compared to the size of the point-spread function (PSF), the cumulant of order n without time-lags can be interpreted as

$$\begin{aligned}\kappa_n(\vec{r}) &\propto \sum_{k=1}^{M} \epsilon_k^n U^n(\vec{r}-\vec{r}_k) f_n(\rho_{\mathrm{on,k}}) \\ &\approx \epsilon^n(\vec{r}) f_n(\rho_{\mathrm{on}};\vec{r}) \sum_{k=1}^{M} U^n(\vec{r}-\vec{r}_k)\end{aligned} \tag{2}$$

with $\epsilon(\vec{r})$ the spatial distribution of the molecular brightness and $\rho_{\mathrm{on}}(\vec{r}) = \frac{\tau_{\mathrm{on}}(\vec{r})}{\tau_{\mathrm{on}}(\vec{r})+\tau_{\mathrm{off}}(\vec{r})}$ the on-time ratio. $U(\vec{r})$ is the system's PSF and $f_n(\rho_{\mathrm{on}};\vec{r})$ is the n-th order cumulant of a Bernoulli distribution with probability ρ_{on}:

$$\begin{aligned} f_1(\rho_{\mathrm{on}};\vec{r}) &= \rho_{\mathrm{on}} \\ f_2(\rho_{\mathrm{on}};\vec{r}) &= \rho_{\mathrm{on}}(1-\rho_{\mathrm{on}}) \\ &\vdots \\ f_n(\rho_{\mathrm{on}};\vec{r}) &= \rho_{\mathrm{on}}(1-\rho_{\mathrm{on}})\frac{\partial f_{n-1}}{\partial \rho_{\mathrm{on}}}\end{aligned} \tag{3}$$

Assuming a uniform spatial distribution of molecules inside a detection volume V centered at $\vec{r}$, we may further approximate

$$\sum_{k=1}^{M} U^n(\vec{r}-\vec{r}_k) \approx \mathcal{E}_V\left\{U^n(\vec{x})\right\} N(\vec{r}), \tag{4}$$

where $\mathcal{E}_V\left\{U^n(\vec{x})\right\} = 1/V \int_V U^n(\vec{x})d\vec{x}$ is the expectation value of $U^n(\vec{x})$ or the n-th moment of $U(\vec{x})$ (see [12] for some examples) and $N(\vec{r})$ denotes the number of molecules within the detection volume V. Finally, we can write

$$\kappa_n(\vec{r}) \approx \mathcal{E}_V\left\{U^n(\vec{x})\right\} N(\vec{r})\epsilon^n(\vec{r}) f_n(\rho_{\mathrm{on}};\vec{r}). \tag{5}$$

Based on at least three different cumulant orders and approximation (5), it is possible to extract the molecular parameter maps $\epsilon(\vec{r})$, $N(\vec{r})$ and $\rho_{\mathrm{on}}(\vec{r})$ by solving an equation system, or by using a fitting procedure. For example, the cumulant orders two to four can be used to build the ratios

$$\begin{aligned} K_1(\vec{r}) &= \frac{\mathcal{E}_V\left\{U^2(\vec{x})\right\}\kappa_3}{\mathcal{E}_V\left\{U^3(\vec{x})\right\}\kappa_2}(\vec{r}) \\ &= \epsilon(\vec{r})\left(1-2\rho_{\mathrm{on}}(\vec{r})\right) \\ K_2(\vec{r}) &= \frac{\mathcal{E}_V\left\{U^2(\vec{x})\right\}\kappa_4}{\mathcal{E}_V\left\{U^4(\vec{x})\right\}\kappa_2}(\vec{r}) \\ &= \epsilon^2(\vec{r})\left(1-6\rho_{\mathrm{on}}(\vec{r})+6\rho_{\mathrm{on}}^2(\vec{r})\right)\end{aligned} \tag{6}$$

and to solve for the molecular brightness

$$\epsilon(\vec{r}) = \sqrt{3K_1^2(\vec{r}) - 2K_2(\vec{r})}, \tag{7}$$

the on-time ratio

$$\rho_{\mathrm{on}}(\vec{r}) = \frac{1}{2} - \frac{K_1(\vec{r})}{2\epsilon(\vec{r})}, \tag{8}$$

and the molecular density

$$N(\vec{r}) = \frac{\kappa_2(\vec{r})}{\epsilon^2(\vec{r})\rho_{\mathrm{on}}(\vec{r})\left(1-\rho_{\mathrm{on}}(\vec{r})\right)}. \tag{9}$$

The spatial resolution of the estimation is limited by the lowest order cumulant, i.e. the second order in this case. However, the presented solution is not unique. Basically any three distinct cumulant orders could have provided a solution. Furthermore, the method is not limited to a two-state system; it can be extended to more states as long as the differences in fluorescence emission are detectable. Additional details on the analytical developments as well as a theoretical investigation of the estimation accuracy of the different parameters under different conditions are given in the Additional file 1.

In order to correct for the amplified brightness and blinking heterogeneities without compromising the resolution, the cumulants have to be deconvolved first. For this purpose, we used a Lucy-Richardson algorithm [13,14] implemented in MATLAB (`deconvlucy`, The MathWorks, Inc.), which is an iterative deconvolution without regularization that computes the most likely object representation given an image with a known PSF and assuming Poisson distributed noise. Apart from the estimate of the cumulant PSF and the specification of a maximum of 100 iterations, all arguments have been left

at their default values. Assuming a perfect deconvolution without regularization, the result could be interpreted as

$$\breve{\kappa}_n(\vec{r}) \approx \epsilon^n(\vec{r}) f_n(\rho_{\mathrm{on}}; \vec{r}) \sum_{k=1}^{M} \delta(\vec{r} - \vec{r}_k). \qquad (10)$$

Taking then the n-th root linearizes the brightness response without cancelling the resolution improvement of the cumulant. To reduce the amplified noise and masking residual deconvolution artefacts, small values (typically $1-5\%$ of the maximum value) are truncated and the image is reconvolved with $U(n\vec{r})$. This leads to a final resolution improvement of almost n-fold compared to the diffraction-limited image, which is physically reasonable since the frequency support of the cumulant-equivalent optical transfer function (OTF) is n-times the support of the system's OTF (cf. [7]). In contrast to Fourier reweighting [7], which is equivalent to a Wiener filter deconvolution and reconvolution with $U(n\vec{r})$, we explicitly split these two steps and use an improved but computationally more expensive deconvolution algorithm that is appropriate for the subsequent linearization.

Since the cumulants are proportional to $f_n(\rho_{\mathrm{on}}; \vec{r})$, which contains n roots for $\rho_{\mathrm{on}} \in [0, 1]$, there might still be hidden image features in these brightness-linearized cumulants (result after deconvolution, n-th root and reconvolution with $U(n\vec{r})$). However, using the on-ratio map $\rho_{\mathrm{on}}(\vec{r})$, it is straightforward to identify the structural gaps around the roots of f_n and fill them in with the brightness-linearized cumulant of order $n-1$. To this end, the locations where f_n approaches zero are translated into a weighting mask with smoothed edges around these locations. The thresholds have been defined by computing the crossing points of $|f_n|^{1/n}$ and $|f_{n-1}|^{1/(n-1)}$. This mask is then applied on the n-th order brightness-linearized cumulant and its negation is applied on order $n-1$ (see Additional file 1 for further details). The result is a balanced cumulant image. It should be noted that the cancellation of $f_n(\vec{r})$ by division is possible but not recommended, because it amplifies noisy structures in the vicinity of the roots of f_n. The combination of multiple cumulant orders in a balanced cumulant image results in a better overall image quality. However, it is also possible that the on-ratio varies only slightly throughout the field of view, such that a combination of multiple cumulant orders is not necessary. Figure 1 illustrates the different steps of the algorithm based on a simulation of randomly blinking fluorophores, arranged in a grid of increasing density from right to left, increasing brightness from left to right and increasing on-time ratio from top to bottom.

Experiments

In order to verify the concept experimentally, we used a custom-designed objective-type total internal reflection (TIR) fluorescence microscope with a high-NA oil-immersion objective (Olympus, APON 60XOTIRFM, NA 1.49, used at 100x magnification), blue (490nm, 8mW, epi-illumination) and red (632nm, 30mW, TIR illumination) laser excitation and an EMCCD detector (Andor Luca S). We imaged fixed HeLa cells with Alexa647-labelled alpha tubulin and used a chemical buffer containing cysteamine and an oxygen-scavenging system [5] (see Additional file 1 for further details) to generate reversible blinking and an increased bleaching stability. The blue laser excitation was used to accelerate the reactivation of dark fluorophores and to reduce the acquisition time. For data processing, 5000 images acquired at 69 frames per second (fps) were divided into 10 subsequences significantly shorter than the bleaching lifetime to avoid correlated dynamics among the fluorophores [10]. The final bSOFI images are obtained by averaging over the processed subsequences.

Results and discussion

Figure 2 compares the performance of bSOFI with conventional SOFI and widefield fluorescence microscopy. The peak signal-to-noise ratio (pSNR; noise measured on the background) in a single frame was 20-23dB for the brightest molecules, which is rather low for performing localization microscopy, but more than sufficient for SOFI [8]. Additionally, we observed significant read-out noise at this acquisition speed (fixed-pattern noise in the average image, Figure 2.**a**,**i**), which was effectively removed in the cross-cumulants analysis (Figure 2.**b-e** and **j**,**k**). The estimated molecular on-time ratio (**c**,**k**), brightness (**d**) and density (**e**) are shown overlaid with the 5th order balanced cumulant as a transparency mask. Due to the overemphasis of slight

heterogeneities in molecular brightness and blinking, the dynamic range of the conventional 5th order SOFI image (**b** and **j**), where values above 1% of the maximum are truncated, is too high to be represented meaningfully. Figures 2.**f**-**h** are the projected profiles of the widefield, SOFI, Fourier reweighted SOFI [7] and bSOFI images along the cuts 1-1', 2-2' and 3-3', respectively. The second profile, with two microtubule structures separated by 80nm, illustrates a situation close to the Rayleigh criteria in the bSOFI case. This is consistent with the measured full width at half maximum (FWHM) of 78nm (Figure 2.**h**). Although the Fourier reweighted SOFI features a FWHM of 75nm (Figure 2.**h**), it does not resolve the two microtubules at 2-2'. Due to the nonlinear brightness response only a single one is visible (Figure 2.**g**). When considering the effective width of the microtubule of 22nm as well as a 15nm linker length, this translates into a bSOFI-equivalent PSF with 64nm FWHM, respectively a 4.6-fold resolution improvement compared to widefield microscopy. The resolution improvement of the conventional 5th order SOFI image is close to the expected factor $\sqrt{5}$. With the red TIR illumination, the excitation intensity decreases exponentially along the optical axis. Assuming a homogeneous illumination in the x-y plane, both the molecular brightness and the on-time ratio can be interpreted as a depth encoding because they are related to the illumination intensity [15]. Obviously, a depth encoding based on molecular parameters can only be used as a qualitative impression of depth information rather than real 3D imaging, because it does not resolve additional structures in depth. Moreover, when looking at smaller scales (Figure 2.**k**), the depth impression of color-coded molecular parameters gets less evident, which can be explained by the influence of local differences in the chemical microenvironment or by the stochastic nature of individual fluorophores.

Although the used Lucy-Richardson deconvolution performed well on our measurements, it is not specifically adapted for cumulant images, because it assumes a Poisson-distributed noise model and an underlying signal that is strictly positive. For the n-th order cumulant, the signal on a single image can vary between positive and negative values according to the underlying on-ratios. Furthermore, initially Poisson-distributed noise leads to a modified noise distribution in the cumulant image. In our experiments, the local on-ratio variations were small, which proves to be unproblematic for a deconvolution with a positivity constraint, when the negative and the positive parts are considered separately. However, a deconvolution algorithm specifically adapted for cumulant images using an appropriate noise model may improve the results of balanced cumulants in the future.

If the cumulants are computed for different sets of time lags and the acquisition rate oversamples the blinking rate, it is also possible to extract absolute estimates on the characteristic lifetimes of the different states. The temporal extent of the curve obtained by computing the second-order cross-cumulant as a function of time lag τ (corresponding to a centred second-order cross-correlation) before it approaches zero yields an estimate on the blinking period, provided that the timeframe of the measurement includes many blinking periods. In our case however, with only 10 to 20 blinking periods within a measurement window of 500 frames (@69fps) and a low on-ratio, the temporal extent of the correlation curve rather corresponds to the characteristic on-time. Figure 3.**a**,**b** show the resulting on- and off-time maps overlaid with a 5th order balanced cumulant as a transparency mask. The reported on-times correspond to the time position where the curve decreased to e^{-1} of the value at zero time lag. The off-time map is obtained by calculating $\tau_{\mathrm{off}} = \tau_{\mathrm{on}} \left(\rho_{\mathrm{on}}^{-1} - 1\right)$. The off-time map hardly shows a dependency on the illumination intensity, which is in line with the deep penetration into the sample of the blue activation light. In the present case, the lifetime of the off-state is influenced mainly by the chemical composition of the microenvironment surrounding the probe [15].

For estimating the average on-time, we computed the second-order cross-cumulant as a function of time lag and averaged it over the x-y-plane and 10 subsequences of 500 frames (Figure 3.**c**). The fitted exponential curve has a characteristic time constant of $\overline{\tau_{\mathrm{on}}} = 31\mathrm{ms}$.

Conclusions

bSOFI is an extended version of SOFI and shares its advantages of simplicity, speed, rejection of noise and background, and compatibility with various blinking conditions. Since the bSOFI-PSF shrinks in all three dimensions with increasing cumulant orders, bSOFI can easily be extended to the axial

dimension by acquiring multiple depth planes and performing the analysis in three dimensions. In contrast to SOFI, the bSOFI response to brightness and blinking heterogeneities in the sample is nearly linear, which allows higher resolutions to be obtained by computing higher cumulant orders. The additional information on the spatial distribution of molecular statistics may be used to monitor static differences and/or dynamic changes of the probe-surrounding microenvironments within cells and thus may enable functional super-resolution imaging with minimum equipment requirements.

Competing interests

The author(s) declare that they have no competing interests.

Author's contributions

SG and CD developed the theory and the algorithm, SG, NB, ML and TL conceived the study, NB and CB prepared the samples, SG and NB performed the experiments and analyzed data, ML and TL supervised the project and SG wrote the manuscript. All authors discussed the results and implications and commented on the manuscript at all stages.

Acknowledgements

This research was supported by the Swiss National Science Foundation (SNSF) under grants CRSII3-125463/1 and 205321-138305/1. The authors would like to thank Prof. Anne Grapin-Botton for the provided infrastructures used for the preparation of the samples and acknowledge Arno Bouwens, Dr. Matthias Geissbuehler, and Dr. Erica Martin-Williams for their constructive comments on the manuscript.

References

1. Huang B, Bates M, Zhuang X: **Super-Resolution Fluorescence Microscopy**. *Annual Review of Biochemistry* 2009, **78**:993–1016.
2. Betzig E, Patterson G, Sougrat R, Lindwasser O, Olenych S, Bonifacino J, Davidson M, Lippincott-Schwartz J, Hess H: **Imaging Intracellular Fluorescent Proteins at Nanometer Resolution**. *Science* 2006, **313**(5793):1642.
3. Hess S, Girirajan T, Mason M: **Ultra-high resolution imaging by fluorescence photoactivation localization microscopy**. *Biophysical Journal* 2006, **91**(11):4258–4272.
4. Rust M, Bates M, Zhuang X: **Sub-diffraction-limit imaging by stochastic optical reconstruction microscopy (STORM)**. *Nature Methods* 2006, **3**(10):793–795.
5. Heilemann M, Van De Linde S, Schüttpelz M, Kasper R, Seefeldt B, Mukherjee A, Tinnefeld P, Sauer M: **Subdiffraction-resolution fluorescence imaging with conventional fluorescent probes**. *Angewandte Chemie International Edition* 2008, **47**(33):6172–6176.
6. Dertinger T, Colyer R, Iyer G, Weiss S, Enderlein J: **Fast, background-free, 3D super-resolution optical fluctuation imaging (SOFI)**. *Proceedings Of The National Academy Of Sciences Of The United States Of America* 2009, **106**(52):22287–22292.
7. Dertinger T, Colyer R, Vogel R, Enderlein J, Weiss S: **Achieving increased resolution and more pixels with Superresolution Optical Fluctuation Imaging (SOFI)**. *Optics Express* 2010, **18**(18):18875–18885.
8. Geissbuehler S, Dellagiacoma C, Lasser T: **Comparison between SOFI and STORM**. *Biomedical Optics Express* 2011, **2**(3):408–420.
9. van de Linde S, Wolter S, Heilemann M, Sauer M: **The effect of photoswitching kinetics and labeling densities on super-resolution fluorescence imaging**. *Journal of Biotechnology* 2010, **149**(4):260–266.
10. Dertinger T, Heilemann M, Vogel R, Sauer M, Weiss S: **Superresolution optical fluctuation imaging with organic dyes**. *Angewandte Chemie International Edition* 2010, **49**(49):9441–9443.
11. Leonov V, Shiryaev A: **On a Method of Calculation of Semi-Invariants**. *Theory of Probability and its Applications* 1959, **4**(3):319–329.
12. Kask P, Gunther R, Axhausen P: **Statistical accuracy in fluorescence fluctuation experiments**. *European Biophysics Journal with Biophysics Letters* 1997, **25**(3):163–169.
13. Richardson W: **Bayesian-Based Iterative Method of Image Restoration**. *Journal of the Optical Society of America* 1972, **62**:55–&.
14. Lucy L: **Iterative Technique for Rectification of Observed Distributions**. *Astronomical Journal* 1974, **79**(6):745–754.
15. van de Linde S, Löschberger A, Klein T, Heidbreder M, Wolter S, Heilemann M, Sauer M: **Direct stochastic optical reconstruction microscopy with standard fluorescent probes**. *Nature Protocols* 2011, **6**(7):991.

Additional Files

Additional file 1 — Theory, algorithm, protocols and estimation accuracies

Additional details on the development of the theory, the algorithm, sample preparation protocols and a theoretical investigation of parameter estimation accuracies.

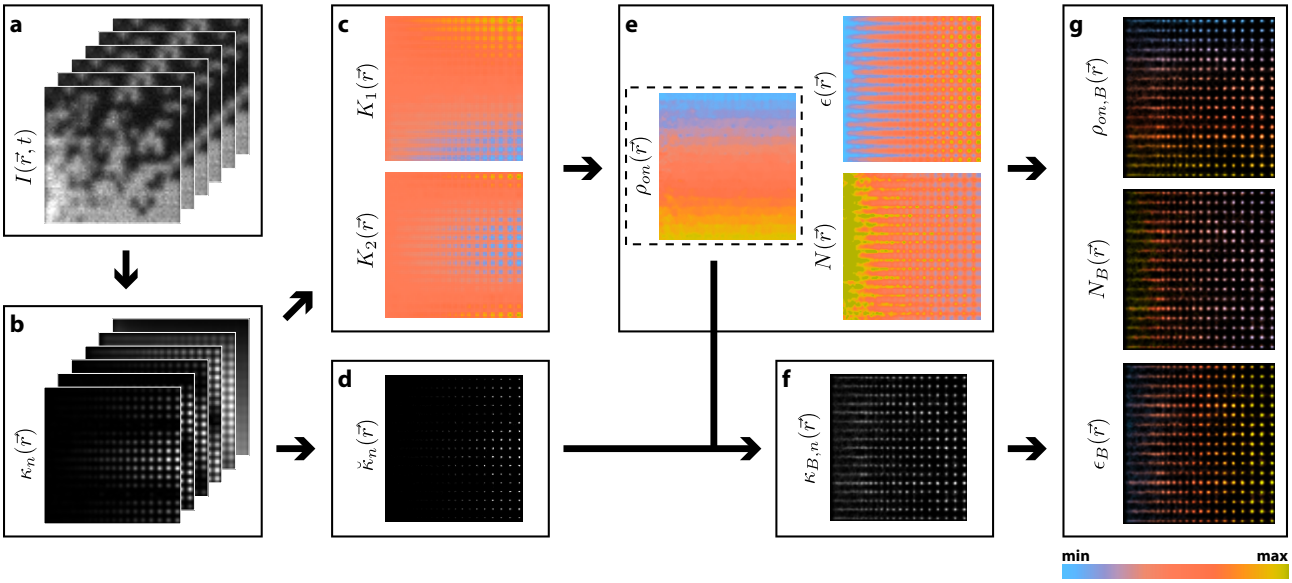

Figure 1: Flowchart to illustrate the different steps of the bSOFI algorithm. (**a**) Raw data. (**b**) Cross-cumulant computation up to order n according to equation (1) without time lags. (**c**) Cumulant ratios K_1 and K_2 according to equation (6). (**d**) Deconvolved cumulant of order n. (**e**) Solution for the spatial distribution of the molecular brightness ϵ, on-time ratio ρ_{on} and density N using equations (7-9). (**f**) Balanced cumulant of order n, obtained by computing the n-th root of the deconvolved cumulant, reconvolving with $U(n\vec{r})$ and filling in the structural gaps around the roots of f_n with a lower-order cumulant. (**g**) Color-coded molecular parameter maps overlaid with a balanced cumulant as a transparency mask.

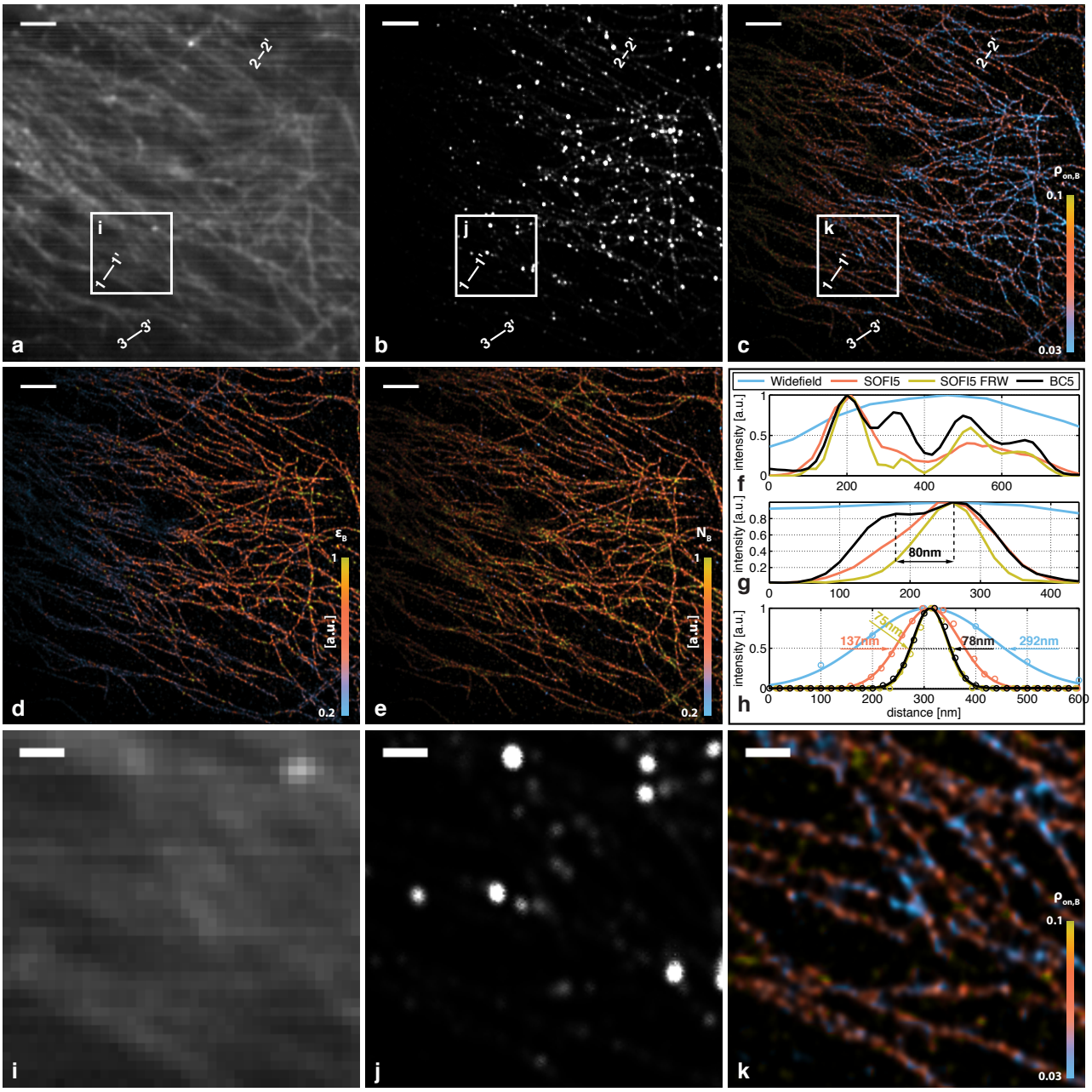

Figure 2: Experimental demonstration of bSOFI on fixed HeLa cells with Alexa647-labelled microtubules. (**a**) Summed TIRF microscopy image [Widefield]. (**b**) Conventional 5th order cross-cumulant SOFI [SOFI5]. (**c-e**) Color-coded molecular on-time ratio, brightness and density overlaid with the 5th order balanced cumulant [BC5]. (**f-h**) Profiles along the cuts 1-1', 2-2' and 3-3'. In yellow we added the corresponding profiles when Fourier reweighting (cf. [7]) with a damping factor of 5% is applied on the 5th order cross-cumulant SOFI image. (**i-k**) Magnified views from the white insets highlighted in (**a-c**). *Scale bars:* $2\mu m$ *(**a-e**);* $500nm$ *(**i-k**)*

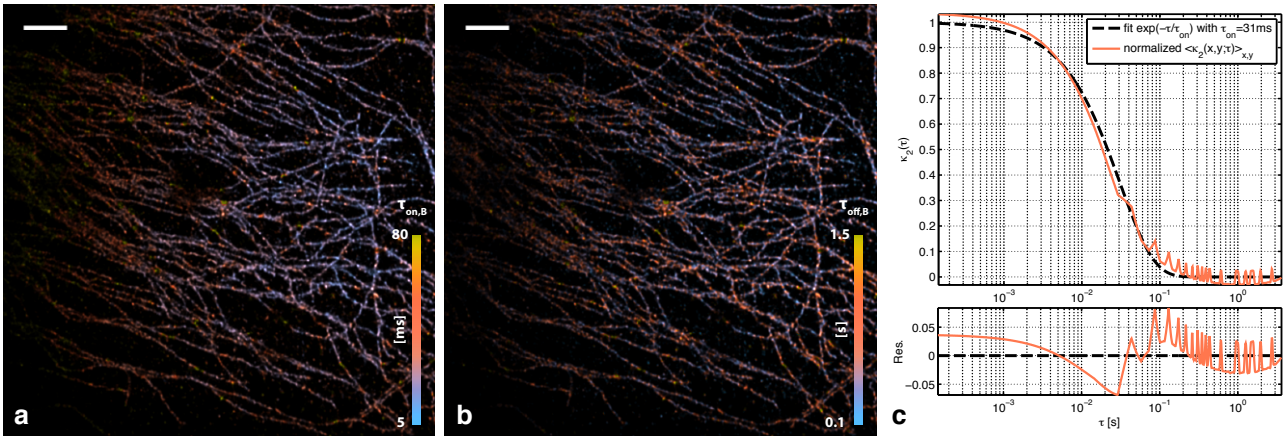

Figure 3: Spatial distribution of the estimated on- (**a**) and off-times (**b**) overlaid with a 5th order balanced cumulant as a transparency mask. The images correspond to an average over 10 subsequences of 500 frames each. (**c**) Second-order cross-cumulant with different time lags, averaged over the x-y-plane and 10 subsequences of 500 frames each. An exponential fit to the measured curve is shown in black. *Scale bars:* $2\mu m$

Additional file 1: Theory, algorithm, protocols and estimation accuracies

Stefan Geissbuehler* , Noelia L Bocchio , Claudio Dellagiacoma , Corinne Berclaz , Marcel Leutenegger and Theo Lasser

Laboratoire d'Optique Biomédicale, École Polytechnique Fédérale de Lausanne, 1015 Lausanne, Switzerland

Email: Stefan Geissbuehler*- stefan.geissbuehler@epfl.ch; Noelia L Bocchio - noelia.bocchio@epfl.ch; Claudio Dellagiacoma - claudio.dellagiacoma@gmail.com; Corinne Berclaz - corinne.berclaz@epfl.ch; Marcel Leutenegger - marcel.leutenegger@epfl.ch; Theo Lasser - theo.lasser@epfl.ch;

*Corresponding author

Theory

The intensity distribution measured over time on a detector pixel $\vec{r}$ of a sample composed of M independently fluctuating emitters can be written as

$$I(\vec{r},t) = \sum_{k=1}^{M} \epsilon_k U\left(\vec{r}-\vec{r}_k\right) s_k(t) + b\left(\vec{r}\right), \tag{1}$$

where ϵ_k, $\vec{r}_k$ and s_k denote the emitter's brightness, its position and its normalized temporal fluctuation signal. $U(\vec{r})$ is the system's point-spread function (PSF) and b represents a temporally constant background term. Taking the n-th order temporal cumulant without time lags leads to

$$\kappa_n(\vec{r}) = \sum_{k=1}^{M} \kappa_n\left\{\epsilon_k U\left(\vec{r}-\vec{r}_k\right) s_k(t)\right\}_t + \kappa_n\left\{b\left(\vec{r}\right)\right\}_t = \sum_{k=1}^{M} \epsilon_k^n U^n(\vec{r}-\vec{r}_k)\omega_{n,k} \tag{2}$$

with $\omega_{n,k} = \kappa_n\left\{s_k(t)\right\}_t$ a weighting factor depending on the blinking properties of the emitter k. If we approximate $U(\vec{r})$ by a Gaussian, $U^n(\vec{r})$ yields a Gaussian PSF with a $\sqrt{n}$-times reduced size in all dimensions leading to a resolution improved by a factor $\sqrt{n}$. Furthermore, applying a simple reweighting scheme in the Fourier domain of the cumulant enables a final resolution improvement that scales linearly with the cumulant order [1].

In addition to structure, higher-order cumulants contain information on the photo-physics of individual emitters. This information is contained in the weighting factors $\omega_{n,k} = \kappa_n\left\{s_k(t)\right\}_t$ and can be extracted by combining several cumulant orders.

In the simplest case, the emitter fluctuates between two states only, i.e. a bright S_{on} and a dark state S_{off}. The relative durations of S_{on} and S_{off}, can be defined as

$$\rho_{\text{on}} = \frac{\tau_{\text{on}}}{\tau_{\text{on}} + \tau_{\text{off}}} \tag{3}$$

$$\rho_{\text{off}} = \frac{\tau_{\text{off}}}{\tau_{\text{on}} + \tau_{\text{off}}} = 1 - \rho_{\text{on}}, \tag{4}$$

where τ_{on} and τ_{off} are the characteristic lifetimes of S_{on} and S_{off}. We may define the fluctuation signal to be 1 when the emitter is in state S_{on} and $\xi \in [0, 1[$ if it is in state S_{off}. The weighting factors $\omega_{n,k}$ then become

$$\begin{aligned}
\omega_{1,k} &= (1-\xi_k)\rho_{\text{on},k} \\
\omega_{2,k} &= (1-\xi_k)^2\rho_{\text{on},k}(1-\rho_{\text{on},k}) \\
\omega_{3,k} &= (1-\xi_k)^3\rho_{\text{on},k}(1-\rho_{\text{on},k})(1-2\rho_{\text{on},k}) \\
\omega_{4,k} &= (1-\xi_k)^4\rho_{\text{on},k}(1-\rho_{\text{on},k})(1-6\rho_{\text{on},k}+6\rho_{\text{on},k}^2) \\
&\vdots \\
\omega_{n,k} &= (1-\xi_k)^n f_n(\rho_{\text{on},k}),
\end{aligned} \tag{5}$$

with $f_n(\rho_{\text{on},k}) = \rho_{\text{on},k}(1-\rho_{\text{on},k})\frac{\partial f_{n-1}}{\partial \rho_{\text{on},k}}$ the n-th order cumulant of a Bernoulli distribution with probability $\rho_{\text{on},k}$.

Since parameters such as the molecular state lifetimes and the molecular brightness often depend on the local environment (for instance the concentration of reducing and oxidizing agents influences the dark-state lifetime of organic fluorophores), we assume region-dependent but locally constant on-time ratios and amplitudes. The overall cumulants can then be approximated by

$$\begin{aligned}
\kappa_1(\vec{r}) &= \widetilde{\epsilon}(\vec{r})\rho_{\text{on}}(\vec{r})\sum_{k=1}^{N} U(\vec{r}-\vec{r}_k) + b(\vec{r}) \approx N(\vec{r})\mathcal{E}_V\left\{U(\vec{x})\right\}\widetilde{\epsilon}(\vec{r})\rho_{\text{on}}(\vec{r}) + b(\vec{r}) \\
\kappa_2(\vec{r}) &\approx N(\vec{r})\mathcal{E}_V\left\{U^2(\vec{x})\right\}\widetilde{\epsilon}^2(\vec{r})\rho_{\text{on}}(\vec{r})\left(1-\rho_{\text{on}}(\vec{r})\right) \\
\kappa_3(\vec{r}) &\approx N(\vec{r})\mathcal{E}_V\left\{U^3(\vec{x})\right\}\widetilde{\epsilon}^3(\vec{r})\rho_{\text{on}}(\vec{r})\left(1-\rho_{\text{on}}(\vec{r})\right)\left(1-2\rho_{\text{on}}(\vec{r})\right) \\
\kappa_4(\vec{r}) &\approx N(\vec{r})\mathcal{E}_V\left\{U^4(\vec{x})\right\}\widetilde{\epsilon}^4(\vec{r})\rho_{\text{on}}(\vec{r})\left(1-\rho_{\text{on}}(\vec{r})\right)\left(1-6\rho_{\text{on}}(\vec{r})+6\rho_{\text{on}}^2(\vec{r})\right) \\
&\vdots \\
\kappa_n(\vec{r}) &\approx N(\vec{r})\mathcal{E}_V\left\{U^n(\vec{x})\right\}\widetilde{\epsilon}^n(\vec{r})f_n(\rho_{\text{on}};\vec{r}),
\end{aligned} \tag{6}$$

where $\mathcal{E}_V\{U^n(\vec{x})\} = 1/V \int_V U^n(\vec{x})d\vec{x}$ is the expectation value of $U^n(\vec{x})$ or the n-th moment of $U(\vec{x})$ (see [2] for some examples) and $N(\vec{r})$ is the number of molecules inside a detection volume V centered at $\vec{r}$. For a 3D Gaussian PSF, the n-th order moment can be written as

$$\mathcal{E}_V\{U^n_{\text{3D Gauss}}(\vec{x})\} = \frac{c(\sigma_{\text{x,y}}, \sigma_z)}{n^{3/2}}, \tag{7}$$

with $c(\sigma_{\text{x,y}}, \sigma_z)$ a constant depending on the spatial extent of the PSF. In our present case, with a total internal reflection (TIR) illumination and a Gaussian approximation of the detection PSF, we find

$$\mathcal{E}_V\{U^n_{\text{TIR Gauss}}(\vec{x})\} = \frac{c(\sigma_{\text{x,y}}, \sigma_z, d_z)}{n^2}, \tag{8}$$

with d_z the characteristic penetration depth of the TIR illumination. Finally we can write

$$\kappa_n(\vec{r}) \approx N(\vec{r})\frac{c(\sigma_{\text{x,y}}, \sigma_z, d_z)}{n^2}\widetilde{\epsilon}^n(\vec{r})f_n(\rho_{\text{on}}; \vec{r}), \tag{9}$$

which enables the pixel-wise estimation of N, $\widetilde{\epsilon}$ (related to the spatial distribution of the average molecular amplitude) and $\rho_{\text{on,off}}$ by considering three or more cumulant orders. To estimate the parameters of a two-state system, the cumulant orders two to four can be used to build the ratios

$$\begin{aligned} K_1(\vec{r}) &= \frac{3^2\kappa_3}{2^2\kappa_2}(\vec{r}) = \widetilde{\epsilon}(\vec{r})\left(1 - 2\rho_{\text{on}}(\vec{r})\right) \\ K_2(\vec{r}) &= \frac{4^2\kappa_4}{2^2\kappa_2}(\vec{r}) = \widetilde{\epsilon}^2(\vec{r})\left(1 - 6\rho_{\text{on}}(\vec{r}) + 6\rho^2_{\text{on}}(\vec{r})\right) \end{aligned} \tag{10}$$

and solving for the amplitude

$$\widetilde{\epsilon}(\vec{r}) = \sqrt{3K_1^2(\vec{r}) - 2K_2(\vec{r})}, \tag{11}$$

the on-time ratio

$$\rho_{\text{on}}(\vec{r}) = \frac{1}{2} - \frac{K_1(\vec{r})}{2\widetilde{\epsilon}(\vec{r})}, \tag{12}$$

and the number of particles

$$N(\vec{r}) = \frac{\kappa_2(\vec{r})}{\widetilde{\epsilon}^2(\vec{r})\rho_{\text{on}}(\vec{r})\left(1 - \rho_{\text{on}}(\vec{r})\right)}. \tag{13}$$

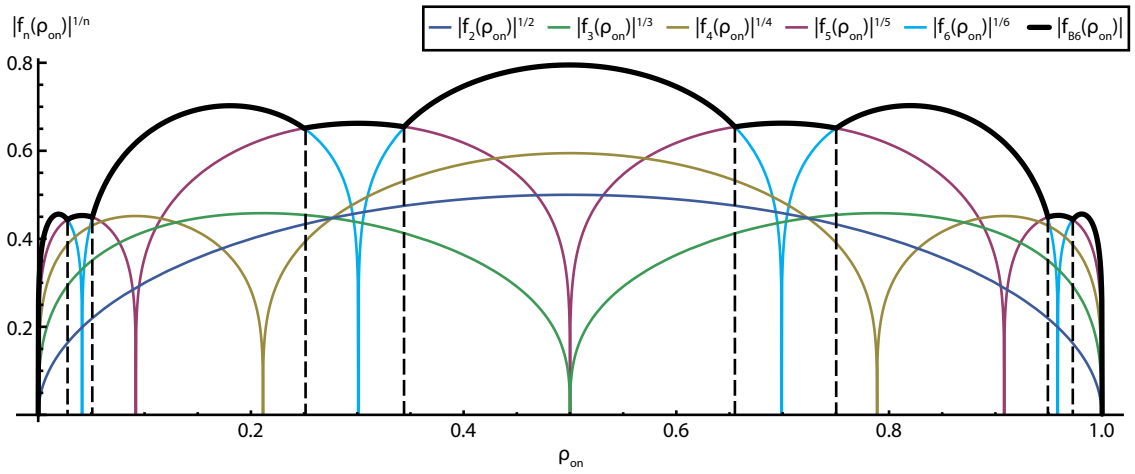

Figure 1: Determination of on-ratio thresholds using $|f_n(\rho_{\text{on}})|^{1/n}$ for combining different cumulant orders (exemplified with the 6th order balanced cumulant in black).

Software

We used a custom MATLAB (The MathWorks, Inc.) code for computing higher-order cross-cumulants according to an algorithm presented previously [3]. For the Lucy-Richardson deconvolution of the resulting cumulants we used the MATLAB implementation `deconvlucy`. The cumulant balancing after deconvolution and brightness linearization involves the combination of cumulant orders n and $n-1$ and first requires an interpolation step to obtain the same number of pixels for both orders. We then used the accordingly interpolated on-ratio map for identifying the image regions exhibiting an $f_n(\vec{r})$ close to zero. The thresholds have been chosen according to Figure 1, where it is shown for the 6th order balanced cumulant.

Estimation accuracy

In order to get an idea on the accuracies of estimating molecular parameters with the proposed method and for a two-state system under different conditions, we implemented a simulation of randomly blinking fluorophores with a certain background offset and Poisson noise evaluated on a single point.

On-ratio estimation

Among all parameters that can be extracted from the data, the estimation of the on-ratio is the most accurate. Figure 2 illustrates the accuracy of the on-ratio estimation for different single molecule peak signal-to-noise ratios (pSNR). Down to a pSNR of only 10dB, the estimation shows reliable results for all $\rho_{\text{on}} \in (0,1)$. At a very low pSNR of 0dB the estimation still works in the range of $0.1 < \rho_{\text{on}} < 0.9$.

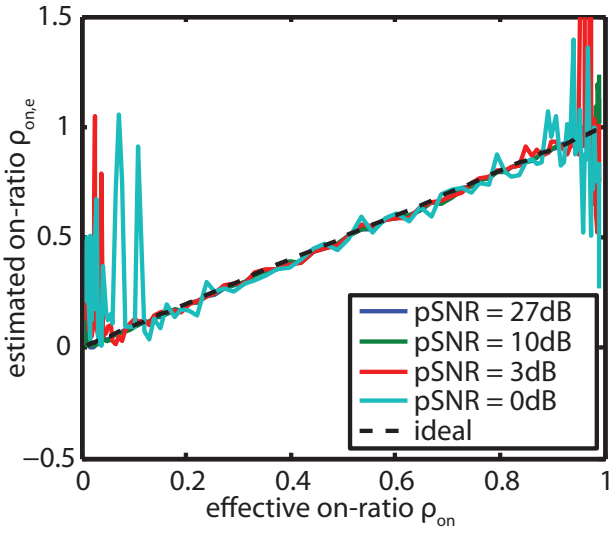

Figure 2: Estimated on-ratio $\rho_{\mathrm{on,e}}$ of a single molecule as a function of the simulated on-ratio ρ_{on} for several pSNRs. Acquisition length: 5000 blinking periods with a temporal double oversampling.

In Figure 3(a) N molecules of equal intensity are hypothetically superposed on the same point. The accuracy of the estimation decreases for a higher number of superposed molecules and improves for low on-ratios. Here, the on-ratio is estimated assuming intentionally and wrongly a 3D molecular distribution and a 3D Gaussian approximation of the PSF (according to equation 8). As the molecules are all located on a single point, this would correspond to a zero-dimensional distribution with $\mathcal{E}\left\{U^n(\vec{r})\right\} = 1$. As a result, there is a small bias barely visible in Figure 3(a) for on-ratios $\rho_{\mathrm{on}} < 0.1$ and $\rho_{\mathrm{on}} > 0.9$.

In Figure 3(b), the additional molecules are uniformly distributed in three dimensions. For more than 10 molecules, the vanishing bias confirmed the correcting moments (equation 8).

Estimation of molecular brightness and density

Figure 4(a) shows the estimation of the brightness in the case of two superposed molecules of different intensities. The simulation demonstrates that the estimated intensity tends towards the value of the brightest molecule. Consequently, the estimation of the absolute number of molecules works well only when the intensities of the molecules are similar at the point of interest (Figure 4(b)). The molecules are counted as long as they are within the detection range with respect to their pSNR. In general, the estimation of the molecular brightness and density is less accurate than the on-ratio estimation and may be used primarily as a qualitative measurement.

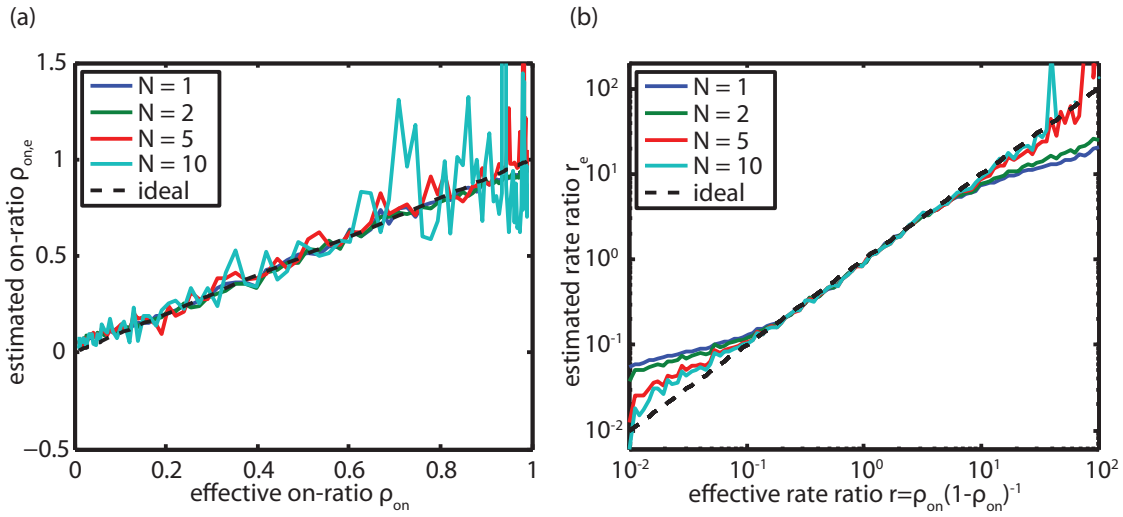

Figure 3: Influence of several superposed molecules on the estimation of the rate ratio **(a)** without and **(b)** with spatial distribution. The on-ratio is estimated using the correcting moments of a 3D PSF (equation 8). **(b)** In the case of a three dimensional molecular distribution, the bias vanishes for more than ≈ 10 molecules.

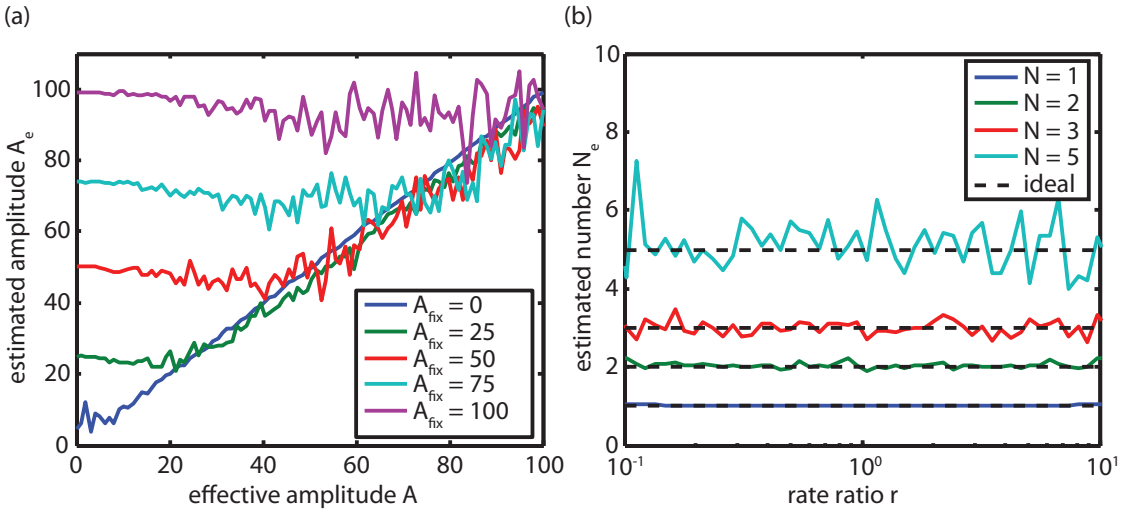

Figure 4: **(a)** Estimation of the molecular brightness A_e for two superposed molecules with the same rate ratio $r = 1$ and different intensities A and A_{fix}. The molecule with the higher intensity is predominant. **(b)** The estimation of the number of molecules N_e of N superposed molecules with equal brightness as a function of the rate ratio.

Protocols

Cell staining

HeLa cells were cultured on glass coverslips. The cells were washed once in PBS prior to fixation with paraformaldehyde (PFA, 4%), and then rinsed 3 times 5 minutes in PBS. The cells were incubated overnight at 4°C with a primary antibody for alpha-tubulin (DM1A, mouse monoclonal, Sigma Aldrich, 1:140) in TBST (Tris-buffered saline and 0.1% Tween20) containing 10% fetal calf serum (FCS).

Cells were washed 3 times 5 minutes in TBST prior to a 2 hours incubation at 4°C with a secondary antibody (donkey anti-mouse, Alexa Fluo 647, diluted 1:400) in TBST containing 10% FCS and washed 3 times 5 minutes in TBST.

The samples were then kept in PBS and stored in the fridge (4°C) for further use.

Imaging buffer

The samples were imaged using a combination of an oxygen scavenger and a thiol. The solutions were prepared using phosphate-buffered saline (PBS) (Sigma Aldrich), 0.5mg/ml glucose oxidase (Sigma Aldrich), 40μg/ml catalase (Sigma Aldrich), 6.6%w/v glucose and 50mM cysteamine (Sigma Aldrich).

References

1. Dertinger T, Colyer R, Vogel R, Enderlein J, Weiss S: **Achieving increased resolution and more pixels with Superresolution Optical Fluctuation Imaging (SOFI)**. *Optics Express* 2010, **18**(18):18875–18885.
2. Kask P, Gunther R, Axhausen P: **Statistical accuracy in fluorescence fluctuation experiments**. *European Biophysics Journal with Biophysics Letters* 1997, **25**(3):163–169.
3. Geissbuehler S, Dellagiacoma C, Lasser T: **Comparison between SOFI and STORM**. *Biomedical Optics Express* 2011, **2**(3):408–420.